

PAPER • OPEN ACCESS

Quantum Otto heat engine based on a multiferroic chain working substance

To cite this article: M Azimi *et al* 2014 *New J. Phys.* **16** 063018

View the [article online](#) for updates and enhancements.

You may also like

- [Efficiency of the non-maximally entangled quantum Otto engine](#)
Heru Sukamto, Lila Yuwana, Agus Purwanto et al.
- [Quantum Otto heat engine with a non-Markovian reservoir](#)
X Y Zhang, X L Huang and X X Yi
- [Nonequilibrium fluctuations of a quantum heat engine](#)
Tobias Denzler, Jonas F G Santos, Eric Lutz et al.

Quantum Otto heat engine based on a multiferroic chain working substance

M Azimi^{1,2}, L Chotorlishvili¹, S K Mishra^{1,3}, T Vekua⁴, W Hübner⁵ and J Berakdar¹

¹Institute of Physics, Martin-Luther University Halle-Wittenberg, D-06099 Halle, Germany

²Max-Planck Institute for Microstructure Physics, Weinberg 2, D-06120 Halle, Germany

³Department of Physics, Indian Institute of Technology, Banaras Hindu University, Varanasi 221005, India

⁴Institute for Theoretical Physics, Leibniz University Hanover, D-30167 Hanover, Germany

⁵Department of Physics and Research Center OPTIMAS, University of Kaiserslautern, PO Box 3049, D-67653 Kaiserslautern, Germany

E-mail: mazimi@mpi-halle.mpg.de

Received 20 January 2014, revised 30 April 2014

Accepted for publication 14 May 2014

Published 12 June 2014

New Journal of Physics **16** (2014) 063018


[doi:10.1088/1367-2630/16/6/063018](https://doi.org/10.1088/1367-2630/16/6/063018)

Abstract

We study a quantum Otto engine operating on the basis of a helical spin-1/2 multiferroic chain with strongly coupled magnetic and ferroelectric order parameters. The presence of a finite spin chirality in the working substance enables steering of the cycle by an external electric field that couples to the electric polarization. We observe a direct connection between the chirality, the entanglement and the efficiency of the engine. An electric-field dependent threshold temperature is identified, above which the pair correlations in the system, as quantified by the thermal entanglement, diminish. In contrast to the pair correlations, the collective many-body thermal entanglement is less sensitive to the electric field, and in the high temperature limit converges to a constant value. We also discuss the correlations between the threshold temperature of the pair entanglement, the spin chirality and the minimum of the fidelities in relation to the electric and magnetic fields. The efficiency of the quantum Otto cycle shows a saturation plateau with increasing electric field amplitude.



Content from this work may be used under the terms of the [Creative Commons Attribution 3.0 licence](https://creativecommons.org/licenses/by/3.0/). Any further distribution of this work must maintain attribution to the author(s) and the title of the work, journal citation and DOI.

 Online supplementary data available from stacks.iop.org/njp/16/063018/mmedia

Keywords: quantum heat engine, quantum entanglement, frustrated spin chain, multiferroic system

1. Introduction

With the advances in nanotechnology enabling controlled miniaturization and functionalization of nanostructured materials, questions related to the thermodynamical properties are gaining increased attention. Several theoretical proposals were put forward for nanoscale Brownian motors [1], refrigerators [2] and quantum heat engines [3–13]. On the other hand, for finite systems, the application of the laws of thermodynamics is the subject of an ongoing debate [14]. One of the fundamental questions concerns the size limit to which the working substance might be scaled down. Recent studies point out that the quantum nature of a size-quantized working substance, e.g. a quantum heat engine, may lead to a close connection between the efficiency of the cycle and quantum correlations [15], which can be quantified in terms of the entanglement [16–18], behavior that is atypical for classical engines. According to the fundamental laws of thermodynamics, the efficiency of a classical engine is independent of its detail and is solely determined by the character of the cycle itself and the temperatures of the heat baths. The quantum nature of the working substance, however, has key consequences for the engine output power as well. Recently it was shown that purely quantum phenomena, such as noise-induced coherence, yield greater engine output power [19, 20].

In general, physical phenomena at the cross-over of quantum mechanics and thermodynamics are the subjects of the emergent field of quantum thermodynamics where, among other topics, questions are addressed as to what extent standard classical thermodynamic cycles, such as Carnot or Otto cycles, can be reformulated for quantum systems [4]. A key issue thereby is the difference between thermodynamic and quantum adiabatic processes. For example, a thermodynamical adiabatic process does not necessarily mean that the occupation probabilities are invariant during an adiabatic transition. As usual, thermodynamical adiabatic processes are identified in terms of the conservation of the entropy and the isolation of the system from the heat exchange with the thermal bath. An essential requirement for the quantum adiabatic process is that the population distributions remain unchanged. Thus, quantum adiabaticity is a stricter requirement than the thermodynamic one. The adiabatic quantum process is also adiabatic in the thermodynamic sense, the opposite is however not true in general. Therefore, quantum adiabaticity entails a relatively low power output from a slowly operating quantum engine, unless the energy spectrum of the working substance has nodal crossing points, however, this is not a generic feature of realistic physical systems. Landau–Zener transitions are avoided during an adiabatic segment of the cycle by slowly varying the control parameters [21]. As mentioned above, the subtlety of quantum engines is related to the internal connection between essentially quantum phenomena such as entanglement and the thermodynamic characteristics of the cycle. In this regard, the choice of the working substance for the operating quantum engine is an important issue [22].

Recently, there has been great interest in composite multiferroic (MF) materials that possess coupled ferromagnetic (FM) and ferroelectric (FE) properties [23–37] (for a review we

refer to [38]). These materials allow for a multitude of novel applications based on the control of magnetism (ferroelectricity) with electric (magnetic) fields. They offer new opportunities for the design and control of new circuits for quantum information processing. For an interesting class of magnetoelectrics, the ME coupling is rooted in a chiral magnetic ordering that is coupled to an electric polarization \mathbf{P} such that [39]

$$\mathbf{P} \sim \mathbf{r}_{i,i+1} \times (\sigma_i \times \sigma_{i+1}). \quad (1)$$

Above $\mathbf{r}_{i,i+1}$ is the relative spatial vector between the effective spins σ_i and σ_{i+1} localized at neighboring sites. Though equation (1) was derived initially phenomenologically, a fully microscopic theory based on the electronic states was developed shortly thereafter [40]. The emergence of an electric polarization, when coupling the spatial degrees of freedom to the spin chirality, renders possible efficient manipulation and control of the spin order parameter via an applied external electric field.

In the present project, we will study a model for a quantum Otto engine operating on the basis of a one-dimensional (1D) finite size MF chiral spin chain that acts as a working substance. The possibility of controlling the efficiency of the quantum heat engine via an external electric field motivates our choice of the working substance. For small working substance consisting of four spins with periodic boundary conditions, we provide an analytical solution to the problem. For a larger size of the working substance an exact numerical diagonalization reveals the connection between the thermal entanglement and the cycle efficiency.

Our theoretical model is experimentally feasible. Recently discovered materials such as the quantum $S = 1/2$ spin chain magnets LiCu_2O_2 , CoCr_2O_4 , LiVCuO_4 , possess simultaneously FE and FM properties. 1D patterns of the chain magnets can be manufactured using CuO_2 powders and a Pt stove [41]. Then, a spin chain magnet doped on the Ir (001) or nonmagnetic Zn^{2+} substrate could serve as a working substance, while a Pt stove could be implemented as a thermal bath for controlling the temperature of the working substance. The cycle we are going to study consists of two thermodynamic adiabatic and two isochoric strokes. During the two isochoric strokes, the MF spin chain interacts with the heat baths. During the two thermodynamic adiabatic strokes the amplitude of the electric field is changed (cf figure 1 for a schematic illustration). Since the energy levels of the system depend on the electric field, a change in the electric field modifies the energy levels. In this way work is done by the engine during the thermodynamic adiabatic strokes. In what follows, we will study the connection between the cycle efficiency, the entanglement and the electric field.

The paper is organized as follows. In section 2 we introduce our model. In section 3 we present analytical results obtained for the MF chain working substance consisting of four spins. In particular we study: the dependence of the pair and the nonlocal many-body entanglements on the temperature and the amplitude of the electric field and the temperature dependence of the quantum chirality and the electric and magnetic susceptibilities. Each of these quantities has a particular meaning: quantum chirality is a measure of the spin frustration and allows to drive the cycle and to control the cycle efficiency by an external electric field. The electric and magnetic susceptibilities can be used to detect the thermal phase transitions in the working substance, and the local and many-body entanglements are useful to observe the connection between the cycle efficiency and the quantum correlations. In section 4 we discuss details of the thermodynamic cycle and in section 5 we evaluate the scaling of the cycle efficiency with the size of the

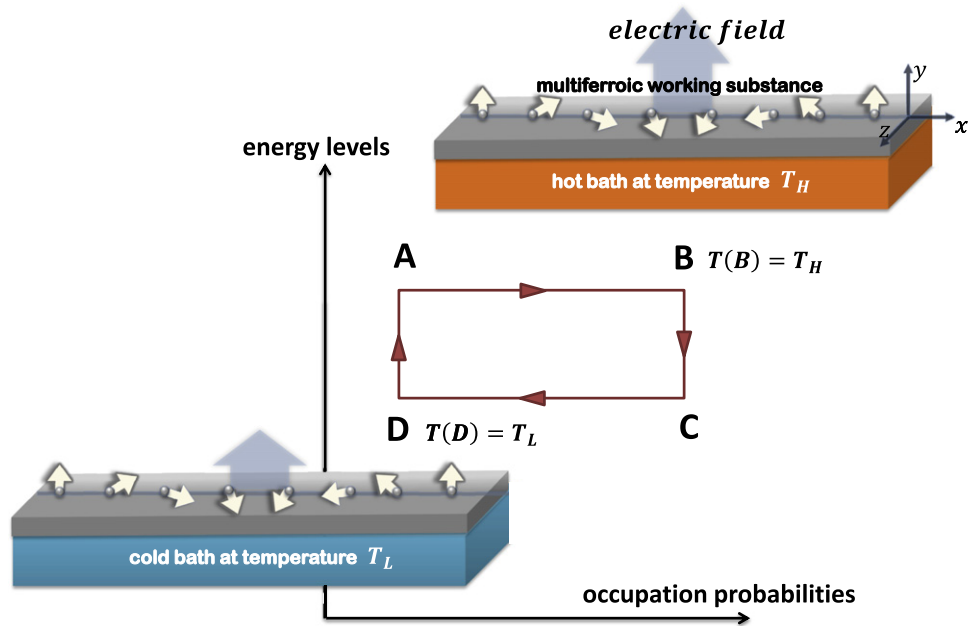


Figure 1. A schematic of the considered quantum Otto cycles based on a chiral multiferroic chain. The cycle has four strokes: steps $A \rightarrow B$ and $C \rightarrow D$ are two isochoric processes. During step $A \rightarrow B$ the system is attached to a hot bath with a temperature T_H . Step $C \rightarrow D$ is inverse to step $A \rightarrow B$. After releasing (absorbing) energy to (from) the cold (hot) heat bath with temperature T_L (T_H) the system reaches a thermodynamic equilibrium state associated with the level populations $P_n^D(E_n(\varphi_1), T_L)$ ($P_n^B(E_n(\varphi), T_H)$). Steps $B \rightarrow C$ and $D \rightarrow A$ are two thermodynamic adiabatic processes. During the process $B \rightarrow C$ the amplitude of the electric field is changed so that $\Delta E_n = E_n(\varphi) - E_n(\varphi_1)$ and the working substance performs positive work.

working substance. In section 6 we study the quantum Otto cycle in the semi-classical limit and wrap up in section 7.

2. Model

We envisage the application of a MF helical chain in one spatial dimension as an electric-field controlled heat engine. For definiteness we take the x axis as the chain direction. An effective model that captures the physics of the MF chain [40, 42] is based on the Hamiltonian

$$\hat{H} = -J_1 \sum_{i=1}^N \sigma_i \cdot \sigma_{i+1} - J_2 \sum_{i=1}^N \sigma_i \cdot \sigma_{i+2} - \gamma_e \hbar B \sum_{i=1}^N \sigma_i^z - \varphi \mathbf{P}. \quad (2)$$

We assumed here that the chain is subjected to an electric field ($\varphi = (0, \varphi, 0)$) applied along the y axis and to a magnetic field B along the z axis. The exchange interaction constant between the nearest neighbor spins is chosen FM $J_1 > 0$ while the next-nearest interaction is antiferromagnetic $J_2 < 0$. Pauli matrices are used in standard notations σ_i , and γ_e is the gyromagnetic ratio for electron spin. \hbar is Planck's constant. With the help of equation (1) the

coupling of the electric field to the MF chain can be written as $\mathcal{E}\mathbf{P} = \mathcal{E}g_{ME} \sum_i (\sigma_i \times \sigma_{i+1})_z$, where g_{ME} is the magnetoelectric coupling strength. The quantity $\kappa_i = (\sigma_i \times \sigma_{i+1})_z$ is known as the z component of the vector chirality (VC) (that we will simply call chirality). Electric field coupling resembles the Dzyaloshinskii–Moriya (DM) anisotropy, with the constant $d = \mathcal{E}g_{ME}$. The effective model Hamiltonian (2) is relevant for 1D spin frustrated MF copper oxides LiCu_2O_2 , CoCr_2O_4 , LiVCuO_4 as discussed in the literature [43–46]. For LiCu_2O_2 the values of the model parameters are $J_1 \approx 81$ K, $J_2 \approx 44$ K, see [45].

The problem of electric-field control of the magnetic chirality of a ferroaxial MF system was addressed in a recent paper [36]. Information transfer by the vector spin chirality in magnetic chains was discussed in [37]. The effect of the electric field or the DM anisotropy variation on the quantum information processing as well as on many-body quantum ground states and quantum-phase transitions of MF helical chain we addressed recently in [42].

In what follows, we suppose that $J_1 = -J_2 = J$ and go over to dimensionless units such that $B \rightarrow \gamma_e \hbar B/J$, $\mathcal{E} \rightarrow g_{ME} |\vec{\mathcal{E}}|/J$, i.e., we measure the Zeeman energy and the interaction energy with electric field in units of the exchange constant. As was mentioned in the introduction, the purpose of the present project is to investigate a possible control of the cycle efficiency and thermal entanglement via an external electric driving field. For clarity we combine analytical and full numerical approaches and start with a solvable model consisting of a four spins with periodic boundary conditions as a working substance.

3. Four spins case: analytical treatment

In the case of four spins, the Hamiltonian (2) can be diagonalized analytically. All technical details are provided as supplementary material (available from stacks.iop.org/njp/16/063018/mmedia). Here we present the main results. To study the thermal entanglement and the cycle efficiency we construct the density matrix $\hat{\rho}$ corresponding to an equilibrium Gibbs distribution,

$$\hat{\rho} = Z^{-1} \sum_{n=1}^{16} \exp[-\beta E_n] |\psi_n\rangle \langle \psi_n|, \quad Z = \sum_{n=1}^{16} \exp[-\beta E_n], \quad (3)$$

where $|\psi_n\rangle$ and E_n are the eigenfunctions and eigenvalues of (2) given explicitly in the supplementary material (see (A1), (A2)). Using the density matrix (3) we calculate the mean value of the z component of the VC. The only nonzero component for the considered configuration of the system and the chosen direction of the electric field is $\langle \sum_{i=1}^4 [\hat{e}_x \times (\sigma_i \times \sigma_{i+1})]_y \rangle = \text{tr}(\hat{\rho} \sum_{i=1}^4 [\hat{e}_x \times (\sigma_i \times \sigma_{i+1})]_y)$, where $\text{tr}(\dots) = \sum_{n=1}^{16} \langle \psi_n | \dots | \psi_n \rangle$.

Following standard definitions [17], we calculate the pair concurrence between two arbitrary spins of the working substance $C_{nm} = \max(0, \sqrt{R_{nm}^{(1)}} - \sqrt{R_{nm}^{(2)}} - \sqrt{R_{nm}^{(3)}} - \sqrt{R_{nm}^{(4)}})$. Here $R_{nm}^{(\alpha)}$, $\alpha = 1, 2, 3, 4$ are the eigenvalues of the matrix $R_{nm} = \rho_{nm}^R (\sigma_1^y \otimes \sigma_2^y) (\rho_{nm}^R)^* (\sigma_1^y \otimes \sigma_2^y)$ and ρ_{nm}^R is the reduced density matrix of the system of two spins obtained from the density matrix of the system $\hat{\rho}$ (3) after tracing out two remaining spins

$\rho_{nm}^R = \text{tr}_{sp}(\hat{\rho})$, where $s, p \neq m, n$. After some rather straightforward calculations we obtain

$$R_{12} = \frac{1}{Z^2} \begin{pmatrix} a_1 d_1 & 0 & 0 & 0 \\ 0 & b_1^2 + |c_1|^2 & 2b_1 c_1 & 0 \\ 0 & 2b_1 c_1^* & b_1^2 + |c_1|^2 & 0 \\ 0 & 0 & 0 & a_1 d_1 \end{pmatrix}. \quad (4)$$

Similarly we calculate for the other components

$$R_{13} = \frac{1}{Z^2} \begin{pmatrix} a_2 b_2 & 0 & 0 & 0 \\ 0 & c_2^2 + |d_2|^2 & 2c_2 d_2 & 0 \\ 0 & 2c_2 d_2^* & c_2^2 + |d_2|^2 & 0 \\ 0 & 0 & 0 & a_2 b_2 \end{pmatrix}, \quad (5)$$

$$R_{14} = \frac{1}{Z^2} \begin{pmatrix} a_1 d_1 & 0 & 0 & 0 \\ 0 & b_1^2 + |c_1|^2 & 2b_1 c_1^* & 0 \\ 0 & 2b_1 c_1 & b_1^2 + |c_1|^2 & 0 \\ 0 & 0 & 0 & a_1 d_1 \end{pmatrix}. \quad (6)$$

In view of equations (4)–(6) for the different pair concurrences we infer

$$\begin{aligned} C_{12} = C_{14} &= \frac{2}{Z} \max \left\{ |c_1| - \sqrt{a_1 d_1}, 0 \right\}, \\ C_{13} &= \frac{2}{Z} \max \left\{ |d_2| - \sqrt{a_2 b_2}, 0 \right\}. \end{aligned} \quad (7)$$

Explicit expressions of the parameters $a_{1,2}$, $b_{1,2}$, $c_{1,2}$, $d_{1,2}$ are quite involved and therefore are presented in the supplementary material (see equations (A3), (A4)). The pair concurrences C_{nm} depend on the chosen spins n and m (more precisely, due to the translational symmetry of periodic chain, on the distance between the two spins) and as one can see from equation (7), C_{nm} are quite different from each other. Therefore, the more informative and universal quantity seems to be the two tangle [47] τ_2 , which contains information on the total pair correlations in the spin chain $\tau_2 = 2C_{12}^2 + C_{13}^2$. Taking into account equation (7) for the two tangle we deduce

$$\begin{aligned} |c_1| > \sqrt{a_1 d_1}, |d_2| > \sqrt{a_2 b_2}: \quad \tau_2 &= \frac{8 \left(|c_1| - \sqrt{a_1 d_1} \right)^2 + 4 \left(|d_2| - \sqrt{a_2 b_2} \right)^2}{Z^2}, \\ |c_1| > \sqrt{a_1 d_1}, |d_2| < \sqrt{a_2 b_2}: \quad \tau_2 &= \frac{8 \left(|c_1| - \sqrt{a_1 d_1} \right)^2}{Z^2}, \\ |c_1| < \sqrt{a_1 d_1}, |d_2| > \sqrt{a_2 b_2}: \quad \tau_2 &= \frac{4 \left(|d_2| - \sqrt{a_2 b_2} \right)^2}{Z^2}, \\ |c_1| < \sqrt{a_1 d_1}, |d_2| < \sqrt{a_2 b_2}: \quad \tau_2 &= 0. \end{aligned} \quad (8)$$

The degree of the pair correlations depends thus on several inequalities between the parameters $a_{1,2}$, $b_{1,2}$, c_1 , $d_{1,2}$, which are functions of the temperature T , and the amplitudes of the driving electric and magnetic fields φ , B . The explicit expressions of the parameters entering equation (8) can be found in the supplementary material as equations (A3) and (A4). In effect, depending on the values of the three parameters φ , B , T the system can be entangled or disentangled. The threshold temperature $T_c(\varphi, B)$ for the given amplitudes of the driving fields defines the regimes of entangled and disentangled states. Our principal interest now is to see how the threshold temperature of the system scales with the electric field $T_c(\varphi)$.

Another interesting object is the one tangle [47] $\tau_1 = 4\det\rho_1$ as it quantifies the nonlocal many-body correlations in the spin chain. Here $\hat{\rho}_1 = \text{tr}_{2,3,4}(\hat{\rho})$ is the reduced density matrix of the first spin after tracing out the states of all other spins. Explicit expressions for the one tangle can be found in the analytical form $\tau_1 = \frac{4}{Z^2}Q$, where the explicit form of Q is presented in the supplementary material (see (A5)). One tangle and the collective nonlocal entanglement is related to the complex spiral spin structure of the frustrated MF chain and therefore is generated by the external electric field. An indication of the existence of the spiral spin structure in the system is the nonzero chirality. Therefore, the values of the z component of the VC $\text{tr}(\hat{\rho}\sum_{i=1}^4[\hat{e}_x \times (\sigma_i \times \sigma_{i+1})]_y)$ and the values of the one tangle $\tau_1 = \frac{4}{Z^2}Q$ are in correlation with each other. Both of them depend on the amplitude of the electric field. Based on the definition of the parameter Q (supplementary material, equation (A5)) it is easy to see that in the high temperature limit $T \rightarrow \infty$ for one tangle we obtain $\tau_1 = 1$. Considering the eigenvalues and eigenfunctions of the Hamiltonian (2) (see supplementary material, equations (A1) and (A2)) for the chirality of the MF chain we obtain:

$$\left\langle \sum_{i=1}^4 [\hat{e}_x \times (\sigma_i \times \sigma_{i+1})]_y \right\rangle = \frac{4}{Z} \left(e^{-\beta E_2} - e^{-\beta E_3} + 8\alpha^2 \mu e^{-\beta E_6} + 8\gamma^2 \lambda e^{-\beta E_7} - e^{-\beta E_{12}} + e^{-\beta E_{13}} \right). \quad (9)$$

The magnetic field dependence of both types of entanglement, namely the short-range pair correlations as quantified by τ_2 and the many-body collective entanglement described by τ_1 , is transparent (this is due to the fact that in our model the magnetic field couples to the magnetization, which is a conserved quantity in our model). With increasing B the entanglements decrease. The dependence on the amplitude of the electric field is less obvious and deserves detailed consideration. First we focus on the thermal pair entanglement τ_2 . As we see in figure 2, τ_2 is finite only for a very large amplitude of the electric field.

The pair thermal concurrence τ_2 is practically zero until the electric field amplitude becomes quite substantial, as can be seen in figure 2 (recall we are operating in scaled units). We also determine the threshold temperature below which τ_2 is finite and above which $\tau_2 = 0$, see figure 3.

In contrast to the pair correlations and the entanglement, the collective entanglement τ_1 is different from zero for an arbitrary electric field (see figure 4).

Another remarkable difference is that the collective entanglement τ_1 is very robust and is practically not affected by the temperature (see figure 5).

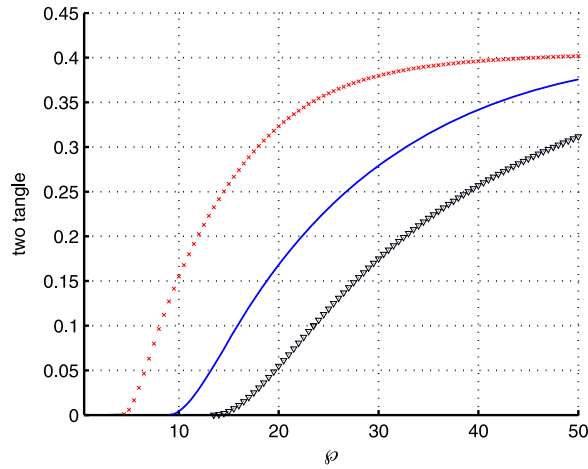


Figure 2. Dependence of the two tangle $\tau_2(\varphi)$ on the electric field for $B = 1$, and for three different temperatures: red cross line $T = 10$, blue solid line $T = 20$, black triangle line $T = 30$.

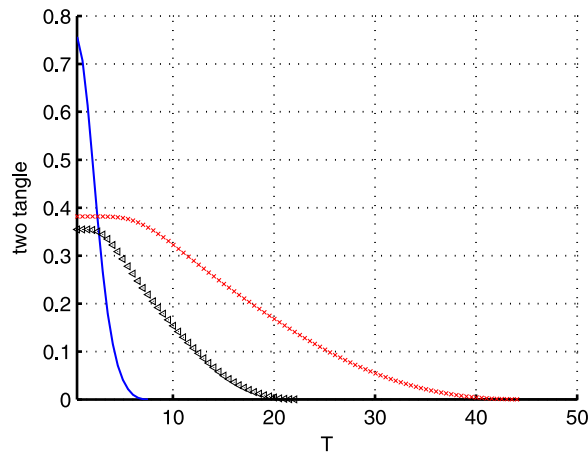


Figure 3. Dependence of the two tangle $\tau_2(T)$ on the temperature for $B = 1$, and for fixed values of the electric field: blue solid line $\varphi = 1$, black triangle line $\varphi = 10$, red cross line $\varphi = 20$. The threshold temperatures are $T_c = 7.37$, $T_c = 22.31$, $T_c = 44.45$, respectively.

Therefore, the amount of thermal entanglement stored in the nonlocal correlations τ_1 is always larger than the thermal entanglement of the pair correlations $\tau_1 > \tau_2$, as shown in figure 6.

With increasing size of the working substance the ratio between τ_2/τ_1 becomes smaller. This means that the many-body entanglement τ_1 is increasing with the size of the system N faster than the total two pair correlations τ_2 . The situation with respect to the thermal chirality is different. In particular, we observe that with increase of temperature the thermal chirality undergoes a strong change and above the threshold temperature T_c of the two tangle τ_2 , the thermal chirality is almost zero, as depicted in figure 7.

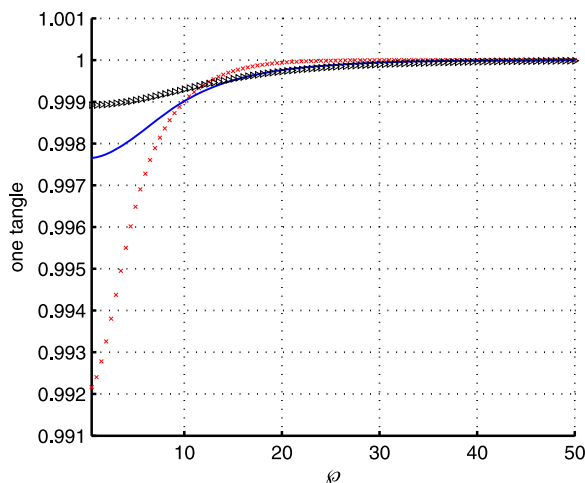


Figure 4. Dependence of the one tangle $\tau_1(\varphi)$ on the electric field for $B = 1$, and for three different temperatures: red cross line $T = 10$, blue solid line $T = 20$, black triangle line $T = 30$.

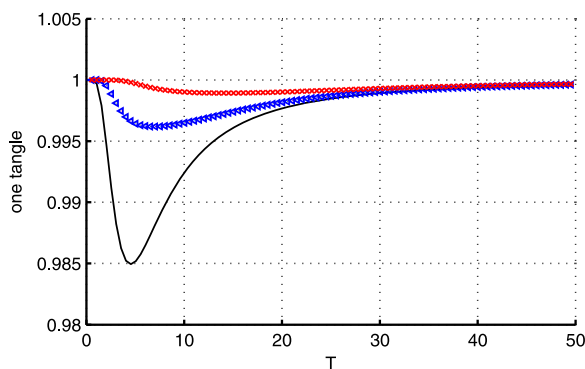


Figure 5. Dependence of the one tangle on the temperature for $B = 1$, and fixed values of the electric field: black solid line $\varphi = 1$, blue triangle line $\varphi = 5$, red cross line $\varphi = 10$.

Thus, we see that the thermal chirality is correlated with the pair correlations in the system. As for the temperature, the magnetic field also has a negative influence on the chirality. The dependence of the thermal chirality on B is plotted in figure 8, where one can see that with increasing B , the thermal chirality decreases.

Another quantity of interest that quantifies the sensitivity to perturbations of quantum systems near a critical region is the fidelity [48]. A zero temperature fidelity is a measure of the overlap between two ground states corresponding to slightly different values of the controlling parameters. A dip in fidelity reflects changes in the structure of the ground state at a quantum critical point [48]. The finite temperature thermal state extension of the quantum fidelity was considered in [49]. The fidelity of a mixed state at a finite temperature characterizes a second-order thermal phase transition [5] and is defined in the following way

$$F_{\zeta}(\beta, \zeta_0, \zeta_1) = \text{tr} \sqrt{\sqrt{\hat{\rho}_0} \hat{\rho}_1 \sqrt{\hat{\rho}_0}}, \quad (10)$$

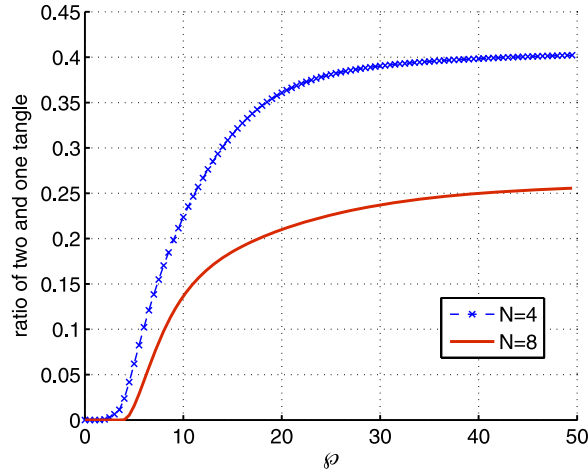


Figure 6. Ratio between two and one tangle τ_2/τ_1 as a function of external electric field for the following values of the parameters $B = 1$, $T = 7.37$. Result for $N = 4$ spins is plotted using obtained analytical solutions. Result for $N = 8$ spins is plotted using numerical solutions.

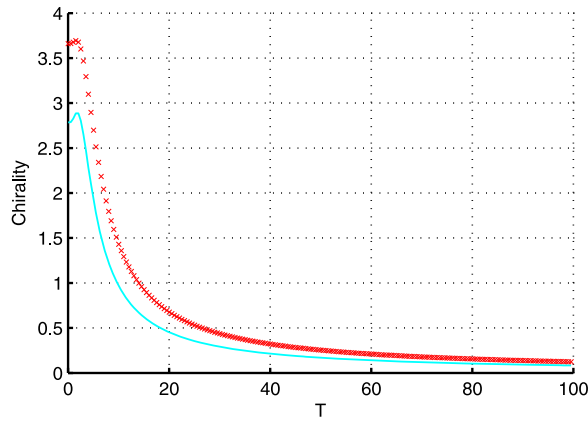


Figure 7. Chirality as a function of the temperature, for $B = 1$, and for fixed values of the electric field: cyan solid line $\varphi = 1$, red cross line $\varphi = 1.5$.

where $\hat{\rho}_0(\beta, \zeta_0)$, $\hat{\rho}_1(\beta, \zeta_1)$ are the density matrices of the system corresponding to slightly different control parameters $\zeta_1 = \zeta_0 + \delta\zeta$ and $\beta = \frac{1}{k_B T}$. The expression for the fidelity related to the electric and magnetic fields can be simplified to the following form

$$F_\zeta(\beta, \zeta, \zeta + \delta\zeta) = \exp\left[-\frac{\beta(\delta\zeta)^2}{8}\chi(\zeta)\right], \quad (11)$$

where $\chi(\zeta) = -\frac{\partial^2 F}{\partial \zeta^2}$ is the susceptibility to the corresponding external field $\zeta = \varphi, B$ at constant temperature. Analytical expressions of the susceptibilities are presented in the supplementary material (equations (A6)–(A7)).

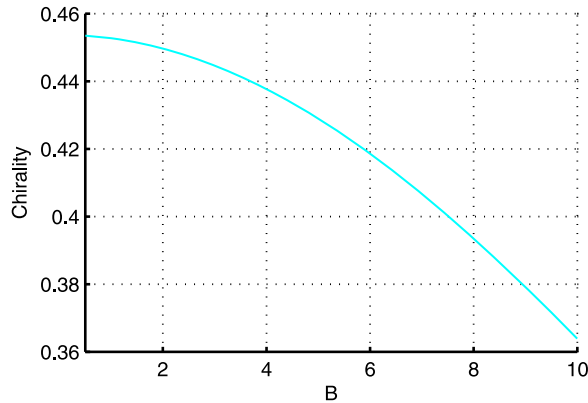


Figure 8. Chirality as a function of the magnetic field for the following values of the parameters $\varphi = 1$, $T = 20$.

Finally, the dependences of the electric $\chi(\varphi)$ and the magnetic $\chi(B)$ susceptibilities on the temperature are depicted in figures 9–12.

According to the definition equation (11), the maxima of the susceptibilities correspond to the minima in the fidelities that are related to the electric and magnetic fields. Comparing figures 9–12 with figure 3, we see a direct correlation between the threshold temperature of the pair entanglement τ_2 and the minima of the fidelities related to the electric and magnetic fields. The maxima of the electric and magnetic susceptibilities are related to threshold temperatures of the pair correlations. For larger threshold temperatures of the pair correlations, the maxima of the electric and magnetic susceptibilities are shifted towards higher temperatures. Interestingly for the electric susceptibility, the correlation between the threshold temperature of the pair entanglement τ_2 and the minimum of the fidelity is not only qualitative but also quantitative as well. As we see for large enough electric fields the maximum of the electric susceptibility is observed almost on the threshold temperatures $T_c \approx 24$, $T_c \approx 45$ of the pair entanglement τ_2 .

In figures 10 and 12 we present the system size dependence of the electric and the magnetic susceptibilities. The heights of the peaks of the electric and the magnetic susceptibilities increase with the system size. One can also observe that for $N = 8$ the location of the peak of the magnetic (electric) susceptibility shifts towards lower (higher) temperatures.

4. Efficiency of the MF heat Otto engine

In analogy to the classical Otto cycle, the quantum Otto cycle also consists of two quantum isochoric and two adiabatic processes [4], as sketched in figure 1. The quantum isochoric process corresponds to heat exchange between the working substance and cold and hot heat baths. During the quantum isochoric process only level populations P_n are reshuffled, while during the adiabatic process the working substance produces work and in this case the energy levels are changed. Therefore, the work produced by the engine depends on the amplitude of electric field, which causes changes in energy levels. An adiabatic process can be thermodynamic adiabatic or quantum adiabatic. A process is thermodynamic adiabatic if the working substance is thermally isolated from the heat exchange with the heat bath. However,

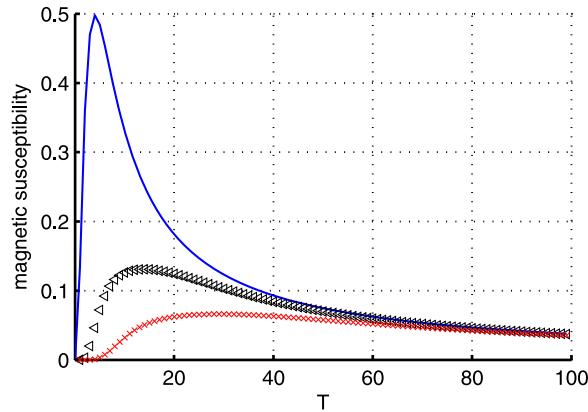


Figure 9. Magnetic susceptibility as a function of temperature for $B = 1$ and for fixed values of the electric field: blue solid line $\varphi = 1$, black triangle line $\varphi = 10$, red cross line $\varphi = 20$. We see that with increasing electric field amplitude the maximum of the magnetic susceptibility is shifted towards higher temperatures.

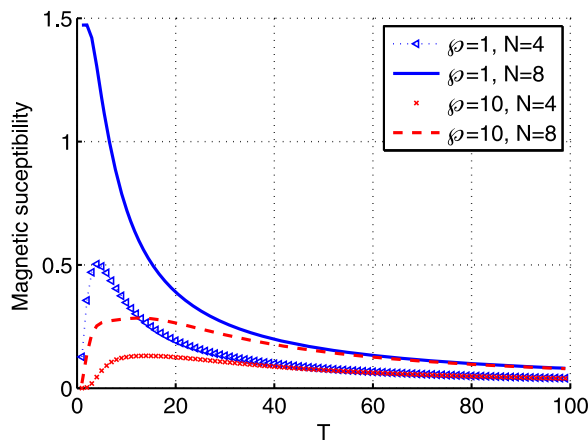


Figure 10. The magnetic susceptibility is plotted as a function of temperature for $N = 4$ and $N = 8$ cases. We choose $B = 1$. The peak in the susceptibility shifts towards lower temperatures as we increase the system size. A similar peak in the magnetic susceptibility at finite temperatures was observed for $B = \varphi = 0$ and $N = 24$ in [50] and was interpreted as the result of a competition between antiferromagnetic and ferromagnetic correlations in the system.

this does not exclude inter-level transitions of a purely quantum nature, while in the case of a quantum adiabatic process the level populations are fixed.

As was mentioned in the introduction, in our case the working substance is a MF spin frustrated chain with a discrete energy spectrum of 16 levels. The first law of thermodynamics for a system with discrete energy spectrum reads

$$dU(E_n, T) = \sum_{n=1}^{16} \left(E_n dP_n + P_n dE_n + E_n \left(\frac{\partial P_n}{\partial E_n} \right)_{T=\text{const}} dE_n \right). \quad (12)$$

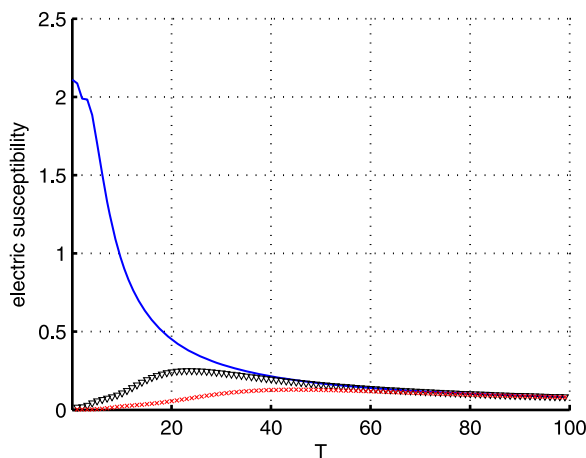


Figure 11. The electric susceptibility as a function of temperature for the following values of the parameters $B = 1$ and for fixed values of the electric field: blue solid line $\varphi = 1$, black triangle line $\varphi = 10$, red cross line $\varphi = 20$. Comparing this result to figure 4 we see that with the increase of the threshold temperature of pair correlations τ_2 the maximum of the electric susceptibility drifts towards higher temperature, $T_c \approx 24$, $T_c \approx 45$.

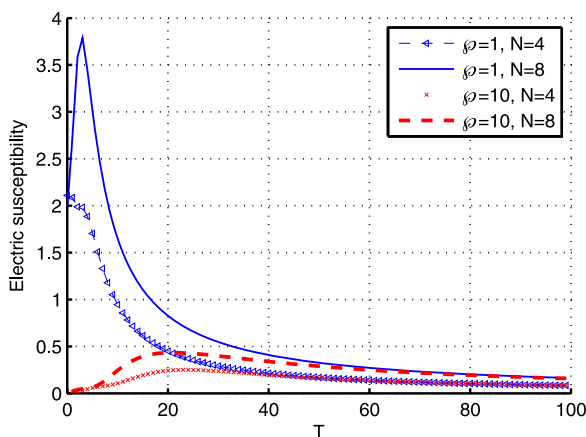


Figure 12. The electric susceptibility as a function of temperature for $N = 4$ and $N = 8$ cases. We set $B = 1$. Note, the electric susceptibility increases as the system size increases.

Here dU is the change of the system energy $U(E_n, T) = \text{tr}(\hat{\rho}\hat{H}) = \sum_{n=1}^{16} E_n P_n(E_n, T)$. The first term on the right-hand side of equation (12), $\delta Q = E_n dP_n$, can be viewed as the heat exchange and is related to the change of the level populations $P_n(E_n, T)$ occurring due to a change of the temperature for $E_n = \text{const}$, while the second and the third terms correspond to the produced work. If the adiabatic strokes of the cycle are quantum adiabatic then $\left(\frac{\partial P_n}{\partial E_n}\right)_{T=\text{const}} = 0$ and equation (12) reduces to the form given in [4]. The work produced during the quantum adiabatic process reads $\delta W = P_n dE_n$. The working substance produces work due to the change of the

amplitude of electric field \wp . This leads to a modification in the energy levels with $\Delta E_n = E_n(\wp) - E_n(\wp_1)$. Our goal is to study the dependence of the cycle efficiency on the modulation of the control parameter, i.e., the electric field amplitude \wp .

To this end we considered two slightly different quantum Otto cycles. As shown in figure 1, the first cycle consists of four strokes [22]: steps A \rightarrow B and C \rightarrow D are two isochoric processes. During the step A \rightarrow B the system couples to the hot bath at temperature T_H and the energy levels are unchanged. After absorbing energy from the hot bath, the system reaches a thermodynamic equilibrium state, which can be described by the level populations $P_n^A(E_n(\wp), T_H)$. Step C \rightarrow D is the reverse of step A \rightarrow B. Namely, the system is brought to couple to a sink at the temperature T_L . After energy exchange with the heat bath a thermodynamic equilibrium state is established, which can be described by the level populations $P_n^D(E_n(\wp_1), T_L)$. Steps B \rightarrow C and D \rightarrow A are quantum adiabatic processes in which the level populations are unchanged, i.e. $P_n^A = P_n^D$, $P_n^B = P_n^C$. During the process B \rightarrow C amplitude of the electric field is changed $\Delta E_n = E_n(\wp) - E_n(\wp_1)$. The working substance performs positive work. Therefore, the heat absorbed by the working substance and the heat released read [22] $Q_{in} = \sum_{n=1}^{16} E_n(\wp) (P_n^B - P_n^A)$, $Q_{out} = \sum_{n=1}^{16} E_n(\wp_1) (P_n^B - P_n^A)$. In the second scenario for the cycle, the quantum adiabatic strokes of the cycle are replaced by thermodynamic adiabatic strokes. The heat absorbed by the working substance Q_{in} and the heat released in the quantum isochoric cooling process Q_{out} in the case of the thermodynamic adiabatic cycle are defined in the following form:

$$\begin{aligned} Q_{in} &= \sum_{n=1}^{16} E_n(\wp) \left(Z^{-1}(T_H, \wp) \exp\left[-\frac{E_n(\wp)}{T_H}\right] - Z^{-1}(T_L, \wp) \exp\left[-\frac{E_n(\wp)}{T_L}\right] \right), \\ Q_{out} &= \sum_{n=1}^{16} E_n(\wp_1) \left(Z^{-1}(T_H, \wp_1) \exp\left[-\frac{E_n(\wp_1)}{T_H}\right] - Z^{-1}(T_L, \wp_1) \exp\left[-\frac{E_n(\wp_1)}{T_L}\right] \right), \end{aligned} \quad (13)$$

while the expression for the cycle efficiency reads

$$\eta = \frac{Q_{in} - Q_{out}}{Q_{in}}. \quad (14)$$

The dependence of the quantum Otto cycle efficiency on the modulation of the electric field amplitude is presented in figure 13.

For both types of cycles (quantum adiabatic and thermodynamic adiabatic) we observed qualitatively similar dependences on the electric field. In both cases the maximal efficiency is reached for certain optimal values of the modulation of the electric field amplitude. However, the maximal efficiency obtained for the thermodynamic adiabatic cycle is higher compared to the efficiency corresponding to the quantum adiabatic case. Let us concentrate on the thermodynamic adiabatic cycle. As one can see reasonably high efficiency of around 75% is achievable already for $\wp/\wp_1 \approx 5$. We also observe a saturation of the cycle efficiency with a further increase of the electric field amplitude. Depending on the amplitude of electric field, the efficiency of the quantum Otto engine might be higher or lower compared to the maximal efficiency of the Carnot cycle $\eta_C = 1 - T_L/T_H$. The reason why the efficiency of

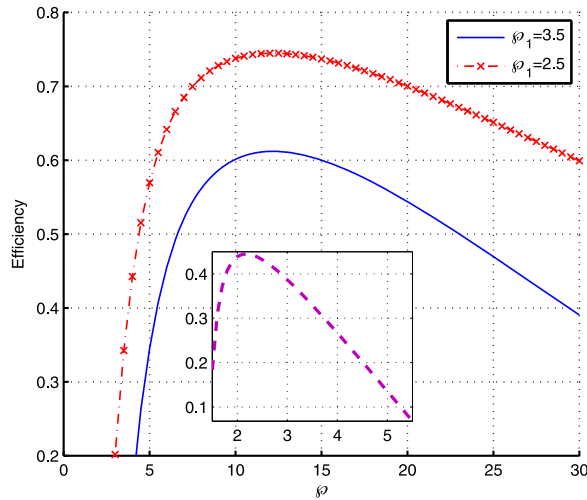


Figure 13. The efficiency of the quantum Otto cycle as a function of the modulation of the electric field amplitude, for the following values of the parameters $B = 1$, $T_H = 30$, $T_L = 10$. The inset corresponds to the quantum adiabatic case. As evident from the figure in the case of a thermodynamic adiabatic quantum Otto cycle, depending on the values of the electric field, the maximal efficiency reaches the value $\eta = 0.75$, which is higher than the maximal efficiency of the Carnot cycle $\eta_C = 1 - T_L/T_H = 0.66$. The efficiency of the quantum adiabatic Otto cycle (inset) is slightly below the efficiency of the thermodynamic adiabatic Otto cycle.

the quantum cycle exceeds the maximal efficiency of the Carnot cycle is of entirely quantum origin, as it can be traced back to the entanglement of the working substance [15]. To illustrate this, we plotted the efficiency of the cycle as a function of the entanglement. Figure 14 evidences that an increase of the entanglement in the system results in enhanced cycle efficiency.

5. Scaling of the cycle efficiency with the size of working substance

In order to investigate the scaling of the Otto cycle efficiency with the size of the working substance for different values of the electric field we plot the dependence of the cycle efficiency on the length of the spin frustrated MF chain N , as shown in figure 15.

The case with a smaller size of the working substance shows different behavior in comparison to a large system size. An abrupt increase in the efficiency is found for $N = 3$. For $N > 4$ the efficiency almost hardly changes with a larger system size. For $N > 4$ and a very high electric field $\varphi = 10$, we encounter the efficiency corresponding to the saturation value.

6. Four spins semi-classical limit

To conclude our analytical considerations we inspect the semi-classical limit utilizing the canonical thermodynamic perturbation theory [51]. We proceed by writing for the

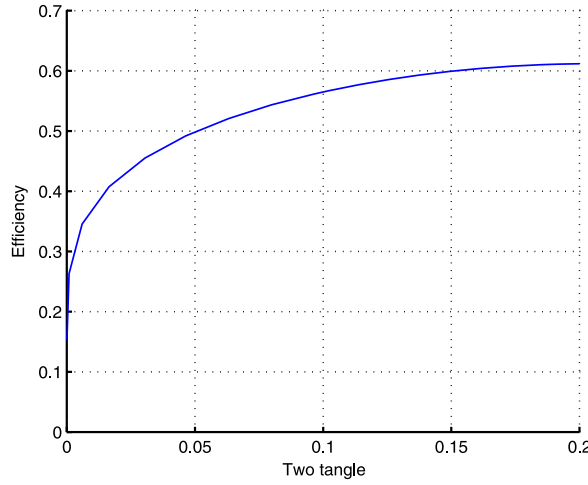


Figure 14. The efficiency of the quantum Otto cycle as a function of the pair entanglement, for the following parameters: $\wp_1 = 3.5$, $B = 1$. We find that strong entanglement in the system is related to enhanced cycle efficiency.

Hamiltonian (2)

$$\begin{aligned}\hat{H} &= \hat{H}_0 + \hat{V}, \\ \hat{H}_0 &= -\sum_{i=1}^N \sigma_i \cdot \sigma_{i+1} + \sum_{i=1}^N \sigma_i \cdot \sigma_{i+2} - B \sum_{i=1}^N \sigma_i^z, \\ \hat{V} &= \wp \sum_i (\sigma_i \times \sigma_{i+1})_z.\end{aligned}\quad (15)$$

Here again $J_1 = -J_2 = J$ ($B \rightarrow \gamma_e \hbar B/J$, $\wp \rightarrow g_{ME} |\vec{\wp}|/J$).

\wp is assumed to be a small parameter. The eigenvalues and the eigenfunction of \hat{H}_0 are denoted by E_n^0 , $|\phi_n\rangle$. We will utilize the normalization condition $\sum_n \exp\left[\frac{F-E_n}{T}\right] = 1$ where $F = -T \ln\left(\sum_n \exp\left[-\frac{E_n}{T}\right]\right)$ is the free energy and the left side of the normalization condition is a function of temperature. Taking the derivative of the normalization condition and after straightforward algebraic manipulations we obtain

$$\Delta F = \left(\frac{\partial F}{\partial T}\right)_{\wp} \delta T + \left\langle \frac{\partial \hat{H}}{\partial \wp} \right\rangle \delta \wp \quad S = -\left(\frac{\partial F}{\partial T}\right)_{\wp}.\quad (16)$$

On the other hand, using the canonical thermodynamic perturbation theory [51] in the semi-classical, high temperature limit $E_n^0 - E_m^0 < T$ we deduce

$$F(T, \wp) = F_0(T, 0) + \langle V(\wp) \rangle - \frac{1}{2T} \left\{ \sum_{m \neq n} \langle |V_{nm}(\wp)|^2 \rangle + \langle (V(\wp) - \langle V(\wp) \rangle)^2 \rangle \right\}.\quad (17)$$

Here $\langle V_{nm}(\wp) \rangle = \sum_n P_n V_{nm}(\wp)$ is the mean value of the matrix element of the perturbation \hat{V} evaluated in the basis of the unperturbed Hamiltonian \hat{H}_0 and $\langle |V_{nm}(\wp)|^2 \rangle = \sum_n P_n |V_{nm}(\wp)|^2$,

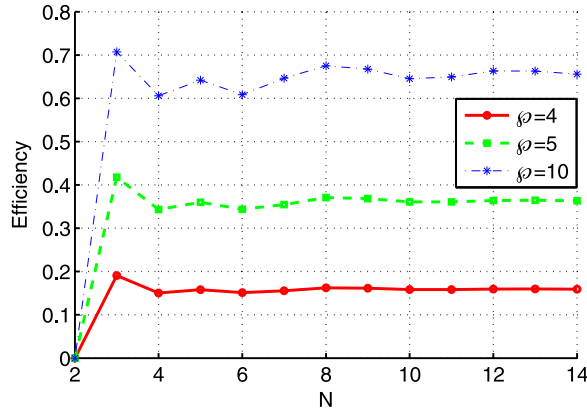


Figure 15. The efficiency for $\varphi_1 = 3.5$ and $\varphi = 4, \varphi = 5, \varphi = 10$ is plotted as a function of system size N . We find that the efficiency jumps abruptly for $N = 3$. For $N > 4$ no significant variation in the efficiency is observed when increasing N . This is observed for all cases.

$\left\langle \left(V(\varphi) - \langle V(\varphi) \rangle \right)^2 \right\rangle = \sum_n P_n \left(V_{nn} - \sum_k P_k V_{kk} \right)^2$. The level populations are described in terms of the Gibbs distribution function P_n . For four spins according to (17) we have

$$F(T, \varphi) = -T \ln \left(\sum_{n=1}^{16} e^{-\frac{E_n^0}{T}} \right) - \frac{16\varphi^2 \left(e^{-\frac{E_2^0}{T}} + e^{-\frac{E_{12}^0}{T}} + e^{-\frac{E_6^0}{T}} + e^{-\frac{E_7^0}{T}} \right)}{T \sum_{n=1}^{16} e^{-\frac{E_n^0}{T}}}, \quad (18)$$

where $E_2^0 = 4J_2 - 2B$, $E_{12}^0 = 4J_2 + 2B$, $E_6^0 = 4J_1 - 4J_2$ and $E_7^0 = 12J_2$. For other energy values of the unperturbed Hamiltonian \hat{H}_0 we refer to the supplementary material. Combining (16) and (17) one can infer that the change in the entropy during the heating and cooling processes depends not only on the initial and the final temperature but also on the electric field. In detail one finds

$$S(T, \varphi) = \ln \left(\sum_{n=1}^{16} e^{-\frac{E_n^0}{T}} \right) + \frac{\sum_{n=1}^{16} E_n^0 e^{-\frac{E_n^0}{T}}}{T \sum_{n=1}^{16} e^{-\frac{E_n^0}{T}}} - 16\varphi^2 \left(\frac{e^{-\frac{E_2^0}{T}} + e^{-\frac{E_{12}^0}{T}} + e^{-\frac{E_6^0}{T}} + e^{-\frac{E_7^0}{T}}}{T^2 \sum_{n=1}^{16} e^{-\frac{E_n^0}{T}}} \right. \\ \left. - \frac{\left(E_2^0 e^{-\frac{E_2^0}{T}} + E_{12}^0 e^{-\frac{E_{12}^0}{T}} + E_6^0 e^{-\frac{E_6^0}{T}} + E_7^0 e^{-\frac{E_7^0}{T}} \right) \sum_{n=1}^{16} e^{-\frac{E_n^0}{T}}}{T^3 \left(\sum_{n=1}^{16} e^{-\frac{E_n^0}{T}} \right)^2} \right. \\ \left. - \frac{\left(e^{-\frac{E_2^0}{T}} + e^{-\frac{E_{12}^0}{T}} + e^{-\frac{E_6^0}{T}} + e^{-\frac{E_7^0}{T}} \right) \sum_{n=1}^{16} E_n^0 e^{-\frac{E_n^0}{T}}}{T^3 \left(\sum_{n=1}^{16} e^{-\frac{E_n^0}{T}} \right)^2} \right). \quad (19)$$

We remark that the entropy is defined by the partial derivative of the free energy with respect to the temperature at constant values of the electric field (16). Therefore, the dependence of the entropy on the electric field is parametrical. If the temperature is constant the entropy is constant, as well. However, the change in the entropy due to a change of the temperature depends on the values of the electric field. equation (19) tells that this dependence is quadratic in the field $S(T, \varphi) - S(T, \varphi = 0) \approx \varphi^2(\dots)$. The entropy as a function of the temperature for different values of the parameters of electric field is plotted in figure 16.

The maximum of the entropy is observed for small values of the electric field and in the high temperature limit. We note that equation (19) is obtained via a thermodynamic perturbation theory and negative values of the entropy correspond to values of the parameters beyond the range where perturbation theory is viable. Taking into account equation (19) we can express the semi-classical efficiency in terms of the electric field as

$$\eta_{sc} = 1 - \frac{\int_{T_L}^{T_H} T \frac{\partial S(T, \varphi)}{\partial T} dT}{\int_{T_L}^{T_H} T \frac{\partial S(T, \varphi_1)}{\partial T} dT}. \quad (20)$$

The semi-classical efficiency as a function of the electric field φ and the temperature difference between the hot and the cold baths $\Delta T = T_H - T_L$ for $T_L = 100$ are presented in figure 17.

The results exhibit larger sensitivity of the semi-classical efficiency to electric field φ than to temperature variations ΔT .

7. Conclusions

In the present project we studied a quantum Otto engine operating with a working substance consisting of electrically controlled MF spin chain. We have shown that due to the existence of a nonzero spin chirality coupled to an emergent electric polarization in the working substance, the efficiency of the cycle is sensitive to the applied external electric field. We analyzed the dependence of the cycle efficiency on the size of the working substance. In particular, for a small working substance consisting of $N = 3$ spins, the efficiency reaches considerably high values, i.e., slightly below 100%. With increasing size of the working substance, the efficiency of the quantum Otto cycle, shows a saturation plateau. Another interesting finding is the robustness of the many-body collective entanglement to temperature variations. Thereby, the many-body entanglement is quantified in terms of one tangle τ_1 and is always larger than the total pair concurrence, as described by the two tangle τ_2 . This indicates that a major amount of the entanglement of the MF working substance is stored in the long-range, multi-spin correlations (see figure 6). In contrast to the one tangle, the pair correlation is sensitive to the increase in the temperature. In particular, we observe the existence of a threshold temperature for the two tangle τ_2 . The stronger the electric field amplitude, the higher is the threshold temperature, as illustrated in figure 3. We encounter the same behavior for the chirality, as well (cf figure 7). In particular, with increasing temperature the thermal chirality undergoes strong changes and for the threshold temperature T_C of the two tangle τ_2 , the thermal chirality reaches its minima. Thus, the thermal chirality is related rather to the pair correlations in the system, not to the nonlocal entanglement. We also studied the relations of the magnetic and the electric

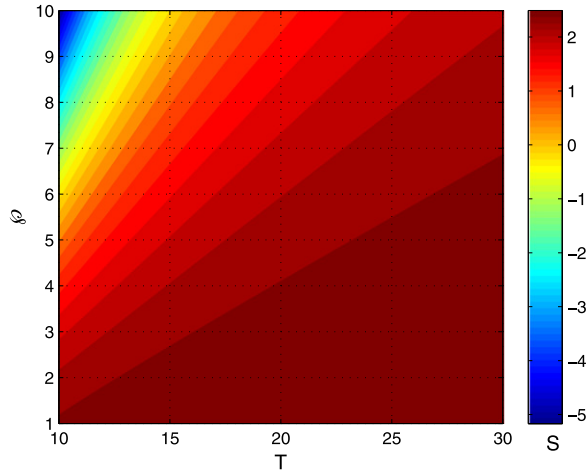


Figure 16. Contour plot of entropy as a function of the modulation of the electric field amplitude and the temperature.

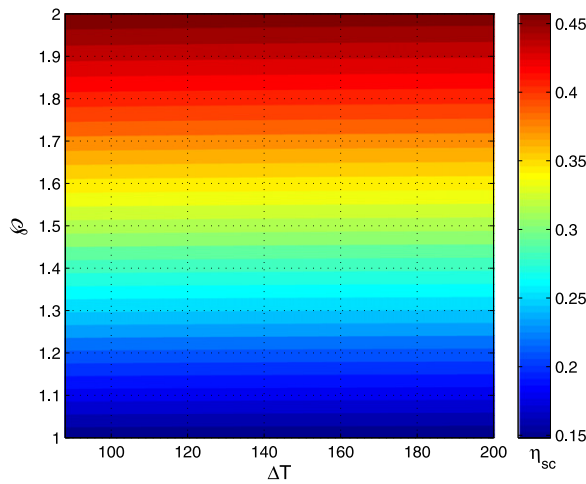


Figure 17. The semi-classical efficiency λ as a function of the electric field φ and the temperature difference between the hot and the cold baths $\Delta T = T_H - T_L$ for $T_L = 100$, $\varphi_1 = 0.5$ plotted using (20). The semi-classical efficiency is more sensitive to the values of the electric field than to the temperature difference ΔT .

susceptibilities to the temperature. According to the definition equation (11), the maximum of the susceptibilities corresponds to a minimum of the fidelity. Comparing figures 9–12 with figure 3, we conclude on a direct correlation between the threshold temperature of the pair entanglement τ_2 and the minimum of the fidelities. The maxima of the electric and the magnetic susceptibilities are related to the corresponding threshold temperatures of the pair correlations. The maximum of the electric susceptibility is observed almost at the threshold temperatures $T_c \approx 24$, $T_c \approx 45$ of the pair entanglement τ_2 . Indeed, the quantum engine with a MF working substance is much more sensitive to the electric field than to the magnetic field, which we think is favorable from an experimental point of view.

Acknowledgments

We gratefully acknowledge valuable discussions with James Anglin. MA, LC, SKM and JB gratefully acknowledge financial support by the Deutsche Forschungsgemeinschaft (DFG) through SFB 762, and contract BE 2161/5-1. TV is supported by QUEST (Center for Quantum Engineering and Space-Time Research) and DFG Research Training Group (Graduiertenkolleg) 1729. WH acknowledges support by Deutsche Forschungsgemeinschaft through SFB-TR 88.

References

- [1] Hänggi P, Marchesoni F and Nori F 2005 *Ann. Phys., Lpz.* **14** 51
Humphrey T E, Newbury R, Taylor R P and Linke H 2002 *Phys. Rev. Lett.* **89** 116801
- [2] Skrzypczyk P, Brunner N, Linden N and Popescu S 2011 *J. Phys. A: Math. Theor.* **44** 492002
- [3] Henrich M J, Mahler G and Michel M 2007 *Phys. Rev. E* **75** 051118
- [4] Quan H T, Liu Y, Sun C P and Nori F 2007 *Phys. Rev. E* **76** 031105
Quan H T, Wang Y D, Liu Y, Sun C P and Nori F 2006 *Phys. Rev. Lett.* **97** 180402
Georgescu I M, Ashhab S and Nori F 2014 *Rev. Mod. Phys.* **86** 153
- [5] Quan H T and Cucchietti F M 2009 *Phys. Rev. E* **79** 031101
- [6] Abah O, Roßnagel J, Jacob G, Deffner S, Schmidt-Kaler F, Singer K and Lutz E 2012 *Phys. Rev. Lett.* **109** 203006
Abah O and Lutz E 2014 *EPL* **106** 20001
Roßnagel J, Abah O, Schmidt-Kaler F, Singer K and Lutz E 2014 *Phys. Rev. Lett.* **112** 03602
Gilz L, Thesing E P and Anglin J R 2013 arXiv:1304.3222
Zagoskin A M, Savelev S, Nori F and Kusmartsev F V 2012 *Phys. Rev. B* **86** 014501
Zagoskin A M, Ilichev E and Nori F 2012 *Phys. Rev. A* **85** 063811
- [7] Linden N, Popescu S and Skrzypczyk P 2010 *Phys. Rev. Lett.* **105** 130401
- [8] Wang R, Wang J, He J and Ma Y 2012 *Phys. Rev. E* **86** 021133
- [9] Jarzynski C 2013 *Phys. Rev. A* **88** 040101
- [10] Deffner S, Jarzynski C and del Campo A 2014 arXiv:1401.1184
- [11] del Campo A, Goold J and Paternostro M 2013 arXiv:1305.3223
- [12] Wang H 2013 *Phys. Scr.* **87** 055009
Van den Broeck C and Lindenberg K 2012 *Phys. Rev. E* **86** 041144
Van den Broeck C, Kumar N and Lindenberg K 2012 *Phys. Rev. Lett.* **108** 210602
- [13] Wang H and Wu G 2012 *Phys. Lett. A* **376** 2209
Esposito M, Kumar N, Lindenberg K and Van den Broeck C 2012 *Phys. Rev. E* **85** 031117
Kumar N, Van den Broeck C, Esposito M and Lindenberg K 2011 *Phys. Rev. E* **84** 051134
- [14] Campisi M, Hänggi P and Talkner P 2011 *Rev. Mod. Phys.* **83** 771
Campisi M 2013 *New J. Phys.* **15** 115008
Campisi M, Blattmann R, Kohler S, Zueco D and Hänggi P 2013 *New J. Phys.* **15** 105028
Joshi D G and Campisi M 2013 *Eur. Phys. J. B* **86** 157
- [15] Dillenschneider R and Lutz E 2009 *Europhys. Lett.* **88** 50003
- [16] Wootters W K 1998 *Phys. Rev. Lett.* **80** 2245
Peuntinger C, Chille V, Mišta L, Korolkova N, Förtsch M, Korger J, Marquardt C and Leuchs G 2013 *Phys. Rev. Lett.* **111** 230506
Usenko V C, Heim B, Peuntinger C, Wittmann C, Marquardt C, Leuchs G and Filip R 2012 *New J. Phys.* **14** 093048

- [17] Amico L, Osterloh A, Plastina F, Fazio R and Palma G M 2004 *Phys. Rev. A* **69** 022304
Amico L, Fazio R, Osterloh A and Vedral V 2008 *Rev. Mod. Phys.* **80** 517
- [18] Mintert F, Carvalho A, Kus M and Buchleitner A 2005 *Phys. Rep.* **415** 207
Lucas F, Mintert F and Buchleitner A 2013 *Phys. Rev. A* **88** 032306
Quijandra F, Porrás D, Garca-Ripoll J J and Zueco D 2013 *Phys. Rev. Lett.* **111** 073602
Reuther G M, Zueco D, Hänggi P and Kohler S 2011 *Phys. Rev. B* **83** 014303
- [19] Scully M O, Chapin K, Dorfman K E, Kim M and Svidzinsky A A 2011 *Proc. Natl Acad. Sci. USA* **108** 15097
- [20] Dorfman K E, Voronine D V, Mukamel S and Scully M O 2013 *Proc. Natl Acad. Sci. USA* **110** 2746
- [21] Shevchenko S N, Ashhab S and Nori F 2010 *Phys. Rep.* **492** 1
Maruyama K, Nori F and Vedral V 2009 *Rev. Mod. Phys.* **81** 1
Buluta I and Nori F 2009 *Science* **326** 108
Wu H, Heinrich G and Marquardt F 2013 *New J. Phys.* **15** 123022
- [22] Wang H, Liu S and He J 2009 *Phys. Rev. E* **79** 041113
Chotorlishvili L, Toklikishvili Z and Berakdar J 2011 *J. Phys. A: Math. Theor.* **44** 165303
- [23] Wang J *et al* 2003 *Science* **299** 1719
- [24] Eerenstein W, Mathur N D and Scott J F 2006 *Nature* **442** 759
- [25] Garcia V *et al* 2010 *Science* **327** 1106
- [26] Bibes M and Barthelemy A 2008 *Nat. Mater.* **7** 425
- [27] Cheong S W and Mostovoy M 2007 *Nat. Mater.* **6** 13
Zhang P, Xiang Z-L and Nori F 2014 *Phys. Rev. B* **89** 115417
- [28] Dawber M, Rube K M and Scott J F 2005 *Rev. Mod. Phys.* **77** 1083
- [29] Valencia S *et al* 2011 *Nat. Mater.* **10** 753
- [30] Duan C-G, Jaswal S S and Tsymbal E Y 2006 *Phys. Rev. Lett.* **97** 047201
- [31] Meyerheim H L, Klimenta F, Ernst A, Mohseni K, Ostanin S, Fechner M, Parihar S, Maznichenko I V, Mertig I and Kirschner J 2011 *Phys. Rev. Lett.* **106** 087203
- [32] Horley P P, Sukhov A, Jia C, Martinez E and Berakdar J 2012 *Phys. Rev. B* **85** 054401
Belinsky M I 2011 *Phys. Rev. B* **84** 064425
Khomskii D I 2010 *J. Phys.: Condens. Matter* **22** 164209
- [33] Sahoo S, Polisetty S, Duan C-G, Jaswal S S, Tsymbal E Y and Binek C 2007 *Phys. Rev. B* **76** 092108
- [34] Kida N and Tokura Y 2012 *J. Magn. Magn. Mater.* **324** 3512
Belinsky M I 2011 *Phys. Rev. B* **84** 064425
- [35] Fechner M, Maznichenko I V, Ostanin S, Ernst A, Henk J and Mertig I 2010 *Phys. Status Solidi B* **247** 1600
- [36] Hearmon A J *et al* 2012 *Phys. Rev. Lett.* **108** 237201
- [37] Menzel M *et al* 2012 *Phys. Rev. Lett.* **108** 197204
- [38] Wang K F, Liu J-M and Ren Z F 2009 *Adv. Phys.* **58** 321–448
- [39] Mostovoy M 2006 *Phys. Rev. Lett.* **96** 067601
- [40] Katsura H, Nagaosa N and Balatsky A V 2005 *Phys. Rev. Lett.* **95** 057205
- [41] Park S, Choi Y J, Zhang C L and Cheong S-W 2007 *Phys. Rev. Lett.* **98** 057601
- [42] Azimi M, Chotorlishvili L, Mishra S K, Greschner S, Vekua T and Berakdar J 2014 *Phys. Rev. B* **89** 024424
- [43] Yamasaki Y, Miyasaka S, Kaneko Y, He J-P, Arima T and Tokura Y 2006 *Phys. Rev. Lett.* **96** 207204
- [44] Rusydi A *et al* 2008 *Appl. Phys. Lett.* **92** 262506
- [45] Yasui Y, Yanagisawa Y, Okazaki R and Terasaki I 2013 *Phys. Rev. B* **87** 054411
- [46] Schrettle F, Krohns S, Lunkenheimer P, Hemberger J, Büttgen N, Krug von Nidda H-A, Prokofiev A V and Loidl A 2008 *Phys. Rev. B* **77** 144101
- [47] Roscilde T, Verrucchi P, Fubini A, Haas S and Tognetti V 2004 *Phys. Rev. Lett.* **93** 167203
Coffman V, Kundu J and Wootters W K 2000 *Phys. Rev. A* **61** 052306
- [48] Zanardi P and Paunkovic N 2006 *Phys. Rev. E* **74** 031123

- [49] Zanardi P, Quan H T, Wang X G and Sun C P 2007 *Phys. Rev. A* **75** 032109
- Paunkovic N, Sacramento P D, Nogueira P, Vieira V R and Dugaev V K 2008 *Phys. Rev. A* **77** 052302
- [50] Heidrich-Meisner F, Honecker A and Vekua T 2006 *Phys. Rev. B* **74** 020403
- [51] Landau L D and Lifshitz E M 1969 *A Course of Theoretical Physics Statistical Physics* vol 5 (Oxford: Pergamon)